

**CFD ANALYSIS OF SUPPRESSION EFFECTS IN A COMMERCIAL  
AIRCRAFT'S TURBOFAN ENGINE****Odenir de Almeida**[odenir.almeida@embraer.com.br](mailto:odenir.almeida@embraer.com.br)

Embraer – Empresa Brasileira de Aeronáutica S.A.

Av. Brigadeiro Faria Lima, 2170 – São José dos Campos S.P – Brazil, 12227-901

**Guilherme Lara de Oliveira**[guilherme.oliveira@embraer.com.br](mailto:guilherme.oliveira@embraer.com.br)

Embraer – Empresa Brasileira de Aeronáutica S.A.

Av. Brigadeiro Faria Lima, 2170 – São José dos Campos S.P – Brazil, 12227-901

**Luis Gustavo Trapp**[gustavo.trapp@embraer.com.br](mailto:gustavo.trapp@embraer.com.br)

Embraer – Empresa Brasileira de Aeronáutica S.A.

Av. Brigadeiro Faria Lima, 2170 – São José dos Campos S.P – Brazil, 12227-901

**Abstract.** *The present work describes the use of CFD tools to investigate the effects of suppression in a turbofan engine of a regional jet aircraft in terms of evaluating the base pressure in the fan cowl trailing edge. Three-dimensional numerical calculations have been performed with two different commercial CFD packages: FLUENT and CFD++. Both software's uses a finite-volume formulation and solves the Navier-Stokes equations on unstructured grids employing improved k-ε turbulent models. The results of numerical calculations in terms of averaged base pressure and Mach number were compared with those from experiments.*

**Keywords.** *CFD, turbofan, aircraft, suppression effects, finite volume*

**1. Introduction**

The aircraft performance is based mainly on data regarding several parameters as drag, lift, cruise speed, weight and specific fuel consumption. However most of these parameters are difficult to evaluate. In fact, the evaluation of the drag and lift forces, for example, can't be measured directly on the system, being obtained, by force balance considering the total thrust and the aircraft weight. While the weight can be evaluated with reasonable accuracy, the in flight thrust determination is still today one of the most challenges and important tasks in the aeronautical industry. There are other reasons for determining drag and hence, thrust in flight, according to literature (Darell Williams, 1996):

- 1) Validation of the analytical model used in aircraft performance prediction;
- 2) Extrapolation of measured performance to untested conditions;
- 3) Demonstration of compliance with contractual requirements;
- 4) Problem identification and rectification of performance shortfalls;
- 5) Identification of components which can be modified to give performance gains for later development of the aircraft;
- 6) Development of the analytical and test technique used in predicting aircraft performance;

In addition, it can be estimated that errors of -1% in the thrust determination during a cruise speed condition could result on +1.12% in variation of fuel consumption of the engine or -1.1% in the aircraft specific range. If a jet airline company operates a hundred of commercial regional aircrafts 2000 hours/year per aircraft, with a fuel consumption of  $6 \times 10^6$  kg/year/aircraft and a fuel price of 0.22 US\$, this order of inaccuracy estimated in thrust determination could represent about 1.5 million of dollars of additional costs for this company. This factor may be determinant in the choice of the aircraft that the passengers companies will operate. It is clear from this simplistic analysis that any reduction in the inherent errors of in-flight thrust determination could reduce drastically costs and represent insertion or not of a new family of airplanes in a competitive market. In fact, new calculus procedures to minimize these errors must be considered by engine and aircraft manufacturer.

It is possible to identify the main difficulties encountered on measurements of in-flight thrust. They are listed below:

- Very tied requirements of measurements accuracy. Typically the errors might be lower than 1%;

- The thrust is measured indirectly taking into account a balance of flow momentum between the exits (nozzles) and the engine intake. This procedure is also obtained by an indirect way based on measurements of thermodynamic parameters like engine's pressure and temperature at different locations. These parameters measurements can vary substantially depending on the location, the available instrumentation and the flow complexity;
- The entire procedure to evaluate the thrust demands laborious previous test bench calibrations of nozzles and isolated engine;
- This whole thrust determination process involves high costs and long time to executing;

Several are the technical issues related to complexity of thrust determination. One of them, very often neglected, is the so called suppression effect. This effect is due to external (freestream) and internal jet flow interaction at the nozzle station and may affect thrust substantially. Actually, the external flow affects the nozzle flow coefficients by a local static pressure change. This flow interaction that only happens in a wind-on configuration, during flight test, may produce a pressure at nozzle that is different of ambient static pressure established during static testing. The changes in nozzle flow coefficients during the test bed affect directly the thrust determination.

The present work describes a numerical method used to investigate the influence of suppression effects in thrust determination of the short-ducted turbofan engine CF34-8E of the newest Embraer EMB-170 regional jet. Three-dimensional calculations have been performed with two different CFD softwares FLUENT and CFD++ which solves the Reynolds averaged Navier-Stokes equations by means of a finite-volume formulation working on unstructured grid. For the turbulence modeling was employed two improved k-ε models: The *realizable* and the *cubic non-linear* one. The results of numerical calculations are based on quantitative parameters as averaged base pressure and Mach number distribution. These results were compared with those obtained from experiments.

## 2. Theoretical Approach

It is known that the thrust experienced by a turbojet is originated by air mass flow momentum throughout the engine, the momentum being the product of mass flow times its velocity. The momentum quantity ( $\dot{M}_0 V_0$ ) is very important in the propulsion theory and its determination on turbofan engines is fundamental for installed performance.

In order to understand the CF34-8E propulsion system, Fig. (1) presents a consistent station numbering of the engine. It is a short-ducted high bypass turbofan engine. The gas generator stream follows the conventional station designation separating the basic cycle processes by intake, compression, heat addition, turbine expansion and nozzle expansion. These stations are identified by the integers 1 through 8. The fan bypass stream utilizes the integer one prefix at each station from the fan ogv (outlet guide vane) to the fan nozzle.

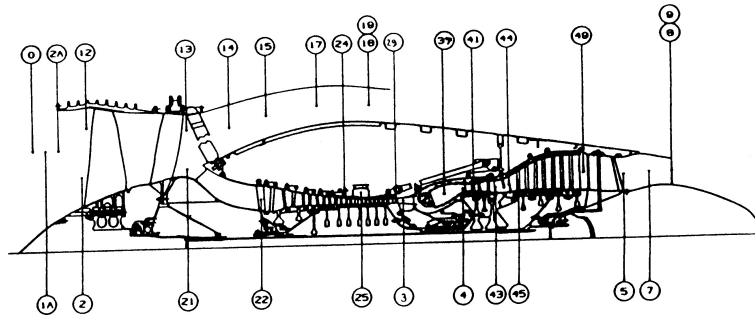


**Figure 1.** The CF34-8E station numbering.

The thrust released by the powerplant is defined as the summation of the forces acting on the internal surfaces of the engine nacelle and pre-entry and post-exit streamtubes. In steady state level flight, with undisturbed flow both far downstream and far upstream of the aircraft, the standard net thrust between stations 0 – 8 and 0 – 19 for the dual stream propulsion system is presented in Fig. (1):

$$F_N = (CF_{G18} \cdot F_{G18} + CF_{G8} \cdot F_{G8}) - F_{RAM} \quad (\text{Net Thrust}) \quad (1)$$

where  $CF_G$  terms are the nozzle thrust coefficients as function of nozzle pressure ratios and:

$$F_{G18} = CF_{18} \cdot \dot{M}_{18} V_{18} + A_{18} (P_{s19} - P_{s0}) \quad (\text{By pass gross thrust}) \quad (2)$$

$$F_8 = CF_9 \cdot \dot{M}_8 V_8 + A_8 (P_{s9} - P_{s0}) \quad (\text{Core gross thrust}) \quad (3)$$

$$F_{RAM} = \dot{M}_0 V_0 \quad (\text{Ram drag}) \quad (4)$$

with  $CF$  terms being nozzle discharge or flow coefficients,  $A$  the nozzle geometrical areas and  $P_s$  the static pressures.

As described in (Santos, 2001) the net thrust may be seen as the vector sum of the ram drag and an appropriate gross thrust term. Thus, the calculation of net thrust is a relatively straightforward process requiring only the knowledge of specific quantities of air mass-flow, velocity and static pressure. What is not so straightforward is the resulting effect of the multitude of variables, always present during any form of jet engine operation, on the specific quantities of air mass-flow and velocity. Since these variable factors affect the performance from which the thrust is derived, they will affect the thrust output. In this case, the concept of base pressure in fan cowls that influences nozzle mass flow and velocity plays an important role on the thrust determination.

In the above expressions  $\dot{M}$  is the ideal mass flow rate, defined based on nozzle pressure and temperature parameters. More details about this formulation are given in SAE Report Air 1703 (SAE, 1985).

$$\dot{M} = \frac{QAP_t}{\sqrt{RT_t}} \begin{cases} \left[ \frac{AP_t}{\sqrt{RT_t}} \cdot \left( \frac{1}{NPR} \right)^{1/\gamma} \sqrt{\frac{2\gamma}{\gamma-1} \left[ 1 - \left( \frac{1}{NPR} \right)^\gamma \right]} \right] & \text{Unchoked Condition} \\ \left[ \frac{AP_t}{\sqrt{RT_t}} \cdot \sqrt{\gamma \left( \frac{2\gamma}{\gamma+1} \right)^{\frac{\gamma+1}{\gamma-1}}} \right] & \text{Choked Condition} \end{cases} \quad (5)$$

where  $Q$  is the so-called mass flow function:

$$\left[ \frac{\dot{M} \sqrt{RT_t}}{AP_t} \right]_{ideal} \quad (\text{Mass flow function}) \quad (6)$$

and  $NPR$  is the nozzle pressure ratio defined as:

$$NPR_{18} = P_{T18} / P_{s\infty} \quad (\text{Fan nozzle pressure ratio}) \quad (7)$$

and

$$NPR_8 = P_{T8} / P_{s\infty} \quad (\text{Core nozzle pressure ratio}) \quad (8)$$

The suppression affects engine performance, mass flow and thrust, basically through the nozzle pressure ratio. In fact, the interaction of nozzles internal and external flows changes the nozzle operating static pressure from ambient ( $P_{s\infty}$ ). This change can only be taken into account either analytically or by means of in-flight measurements of the nozzles operating pressures ( $P_{s19}$  and  $P_{s9}$ ). The second option is very often discarded due to pressure parts instrumentation difficulties.

It's still important to emphasize that the degree of suppression is extremely nacelle configuration and installation dependent, and may vary with free stream Mach number, wing flap setting configuration and the aircraft angle of attack in an underwing engine installation.

In this work this suppression effect will be estimated numerically with two different CFD codes and the results compared to engine manufacturer experimental data.

### 3. Suppression Estimation Methods Background

As described in SAE Report Air 1703, in aircraft design there are some methods used to account for fan suppression of core nozzle coefficients and external-flow suppression of fan nozzle coefficients. The use of scale-model tests has generally been used in the thrust validation process. Pressure measurements have been made on full-scale aircraft in flight and compared with those ones from tunnel tests. This technique would require the measurement of the nozzle base pressures. In this case, nozzle base static pressures,  $P_{s9}$  and  $P_{s19}$  substitutes the free-stream ambient pressure

in the nozzle pressure ratio, used to characterize the coefficients. These measurements may reveal problem areas related to flow interaction such as severe flow separation and consequent sources of drag. Results from these pressure-measurement tests can lead to re-shaping the nacelle surfaces. In wind tunnel cases, very careful attention must be paid to the scaling of all the geometrical surfaces, particularly in complicated designs. Consideration of scale and boundary layer effects on the force field is advisable. Any differences between scale-model and full-scale reference areas or pressure ratios must be accounted too.

In spite of reliability and maintainability of these experimental techniques they are sometimes very expensive and require hours of test calibration, in-flight and tunnel. On the other hand more modern methods have been proposed to account for suppression in aeronautical applications. A large number of these methods are based on evaluating empirical equations and correlations. By the other hand, a notable growing has been seen on the development of new CFD tools capable of predicting accurately the nozzle base pressure. This numerical approach has become more interesting since the availability of large computing power, new developments in grid generation and algorithms and also due the lower general cost when compared to an in-flight and wind tunnel tests.

Nowadays in the aeronautical industry it seems to be entirely possible to compute tridimensional flow past airplanes with some reasonable accuracy employing Reynolds-Averaged Navier-Stokes equations and different mesh discretizations, in accordance to (Tularpurkara, 1997).

#### 4. CFD Analysis

For some kind of analysis, nacelles and airframe are considered to be decoupled. This idealized assumption is useful to CFD analysis since this permits the retention of a simpler CFD analysis in terms of domain size and time computing. This is the case for the work herein presented. Basically, this simplification implies that the flow field of the airframe has little influence on nacelle external flow.

##### 4.1. Unstructured Mesh Application

The computations simulate the full-scale CF34-8E nacelle. This is a short-duct nacelle composed by an inlet, fan cowl, aft core cowl and plug. Figure 2 shows the whole domain used in calculations and details of the unstructured hexahedral mesh of the nacelle.

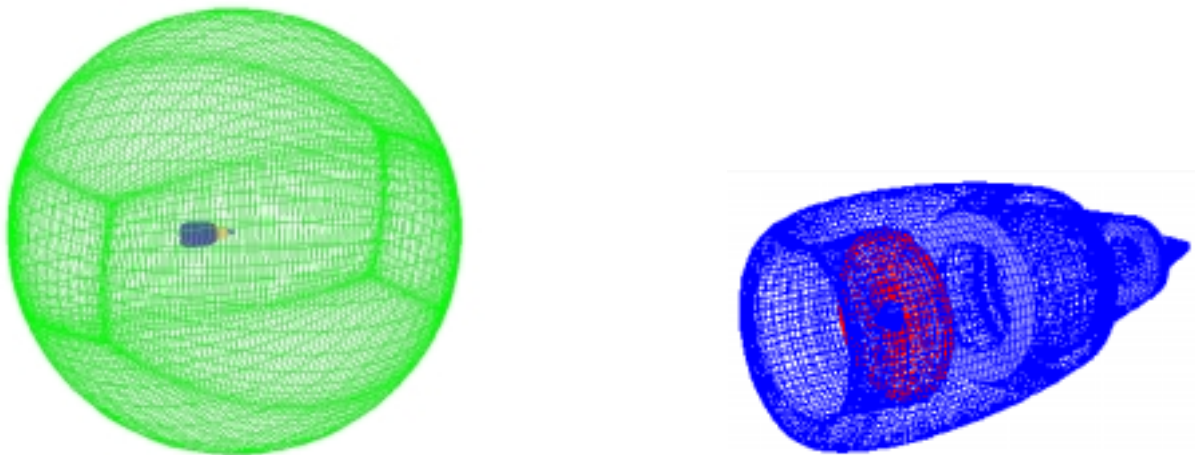


**Figure 2.** Computational domain and nacelle's mesh.

The computational grid consists of 873.791 hexahedral cells. The highlite diameter of the intake's engine ( $D_H$ ) has been used as characteristic length for the diameter of the sphere used as farfield (about  $20D_H$  upstream and  $30D_H$  downstream). A refined mesh near the wall has been used to increase the accuracy of results in terms of capture of shock waves and flow gradients. This results in  $y^+$  values of the order of 30 for the first grid point off the surface. It is important to emphasize that this near-wall approach, associated to  $k-\epsilon$  modeling used, has provided some reasonable results for this kind of problem. The maximum grid-stretching ratio in all directions is limited to 1.2 to guarantee uniformity and reasonable finite volume approximation in the entire grid. The leading and trailing edge of the fan cowl has been discretized with 40 node points. A minimum of 10 nodes was included inside the boundary layer.

##### 4.2. CFD Flow Solvers

The flow calculations presented here were performed with two different commercial codes: FLUENT v5.6.4 and CFD++ v3.2. Both codes solves the three dimensional steady compressible form of the Reynolds-Averaged Navier-Stokes equations by means of a finite volume formulation with turbulence models.

In both solvers it is utilized a turbulence modeling based on improved k-ε models. In simulations with FLUENT it has been used the k-ε *realizable* model. This model proposed by Shih *et al.* (1995) was intended to improve some deficiencies in the k-ε standard model, as a fundamental defect to neglect rotation, anisotropy and non-equilibrium effects. Basically in this model two important characteristics were incorporated. A new eddy-viscosity formula involving a variable  $C_{\mu}$  originally proposed by Reynolds (1987) and a new model equation for dissipation ( $\epsilon$ ) based on the dynamic equation of the mean-square vorticity fluctuation. More details are provided in Shih *et al.* (1995).

The CFD++ solver has implemented the k-ε *cubic* model. This improved k-ε model extends the linear k-ε model with quadratic terms by Shih *et al.* (1993) and cubic terms by Lien & Leschziner (1996). The former yield an anisotropic representation of the normal stresses, the latter account for streamline curvature and swirl effects. This model works very well in all but the hypersonic flow regime and has been documented to predict by-pass transition in both low and high speed flows. It is currently the default model in CFD++. Details are given in Goldberg *et al.* (1999).

All simulations were ran in a Silicon Graphics machine with 1 CPU taking about 24 hours for each residual convergence. The residual plots have dropped about 4 orders of magnitude. This convergence rate is fairly typical of all runs.

### 4.3. Conditions Analyzed

Table 1 shows the flight conditions analyzed in this study. In this preliminary investigation, only four different cases were proposed to evaluate the external flow suppression effects based on Embraer requirements of performance.

**Table 1.** Flight conditions proposed to analysis.

	Engine Rating*	Altitude (ft)	Mach number	Fan NPR	Nacelle Angle of attack
Case 1	82.3	15000	0.4	1.545	0°
Case 2	68.8	15000	0.6	1.543	
Case 3	72.6	25000	0.7	1.730	
Case 4	65.8	35000	0.7	1.629	

\* Percent corrected fan speed (%7000 rpm) for any flight condition within the flight envelope.

### 4.4. Boundary Conditions

The numerical boundary conditions used to describe the engine operation are shown schematically in Fig. (3) These boundary conditions were taken from a previous numerical calculus of CF34-8E steady-state performance, computed from the thermodynamic cycle deck of the engine (so-called DECK program).

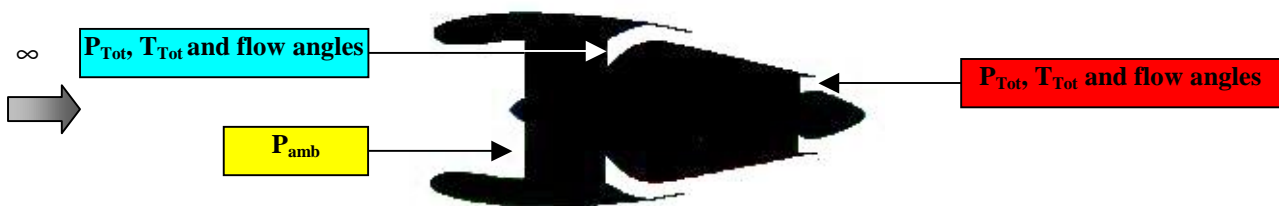


**Figure 3.** Boundary conditions applied to the engine.

### 4.5. Calculus procedure of suppression effects by CFD

The block diagram shown in the Figure 4 contains the summary of the calculus and post-processing procedure to account for suppression effects. This procedure uses data from the thermodynamic cycle of engine and results obtained from CFD analysis.

**Step 1:** For each case of Table 1 it is necessary to run the thermodynamic cycle of the engine to obtain the fan nozzle pressure ratio ( $NPR_{18}$ ) and the fan exhaust nozzle flow coefficient ( $CF_{18}$ ) at station 18. On the other hand the CFD calculus provides the average nozzle operating static pressure at fan cowl trailing edge ( $P_{sb19}$ ). The suppression effects are evaluated in terms of change in the  $NPR_{18}$  taking into account the ( $P_{sb19}$ ), different of ambient value, provided by CFD, i.e.  $NPR_b$ .

**Step 2:** The thermodynamic cycle of the engine is run again for several rating of powers. To do this, the DECK program is run varying the thrust in terms of fan percentage of speed ( $N_1$ ). This process is cyclic until the new value of nozzle pressure ratio ( $NPR_b$ ) is achieved. Provided convergence of this DECK procedure, the corrected fan exhaust nozzle flow coefficient ( $CF_{18corrected}$ ) is determined.

**Step 3:** In this step it is evaluated the non-dimensional expression of the flow function ( $Q$ ) considering if the nozzle is or not choked. Finally the suppression effects are estimated in terms of percentage of flow function times fan exhaust nozzle flow coefficient  $\Delta(Q \times CF_{18})$ .

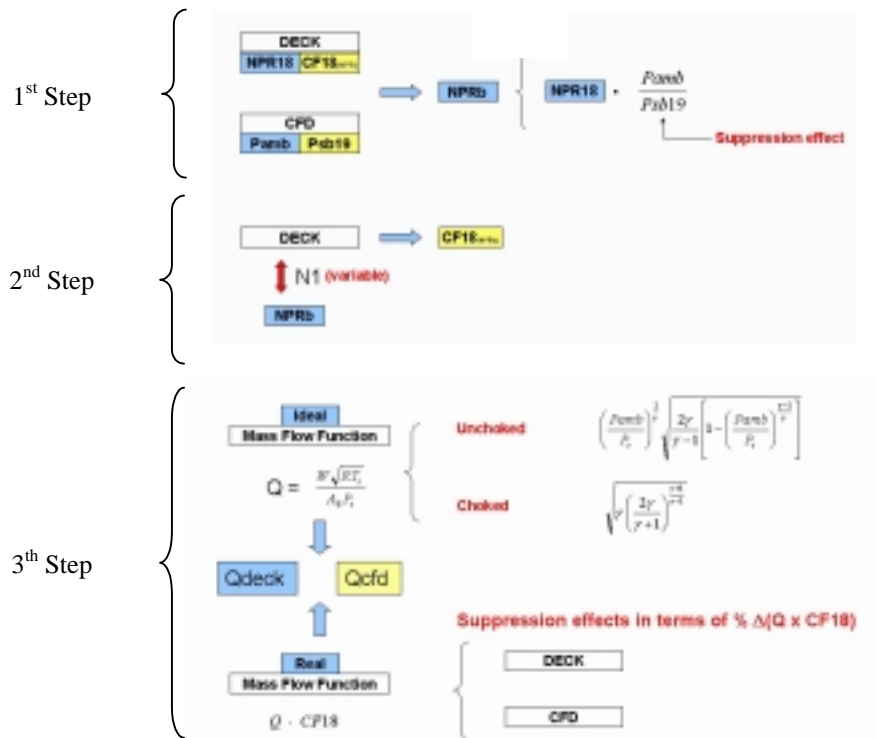


**Figure 4.** Block diagram of suppression calculus.

## 5. Numerical and Experimental Results

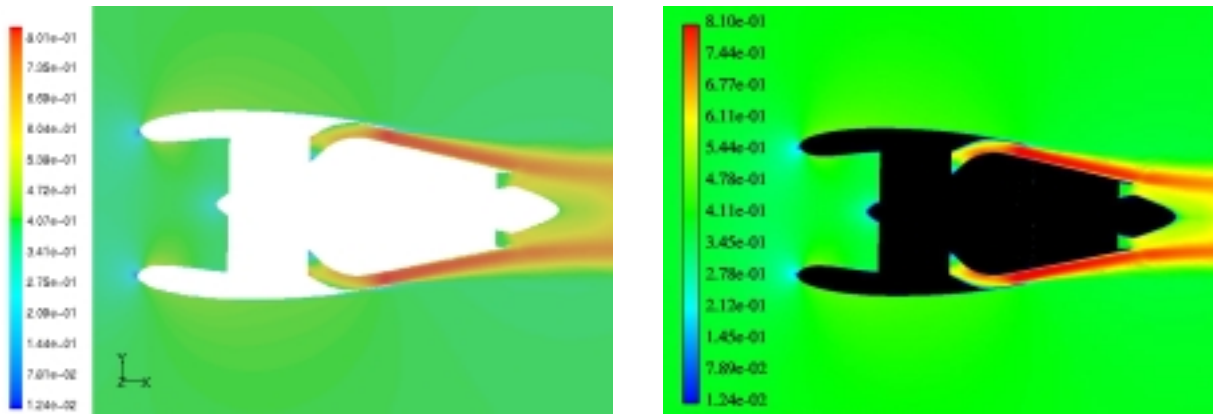
The results presented herein compare the numerical predictions of the two different codes employed. The Mach number and static pressure flow fields are firstly shown. The average static base pressure at the fan cowl trailing-edge are then presented. The analysis of Mach number field is used to identify possible detachments points and shock waves over the nacelle. The results of suppression effects are compared with those experimental from engine manufacturer.

### 5.1. Mach number field

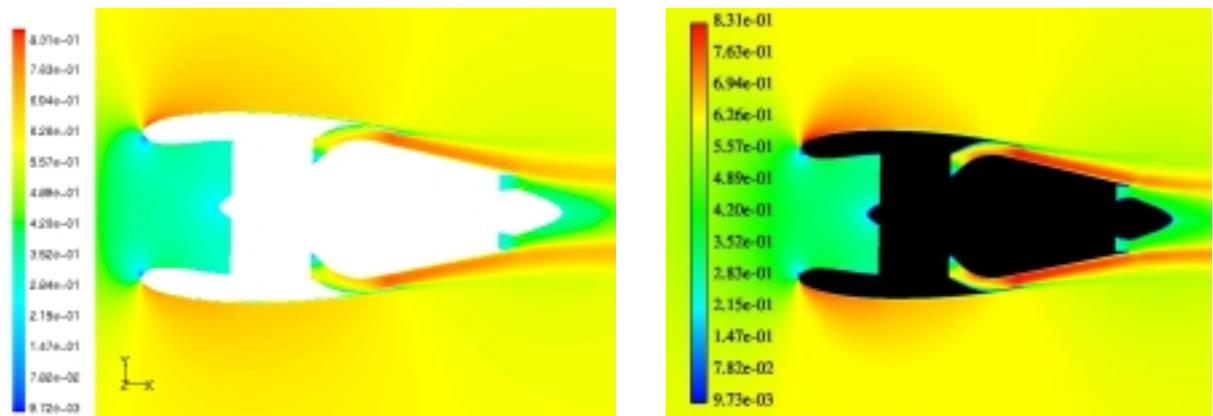
Figure 5 presents results of Mach number obtained with the two CFD packages used. The Mach number fields have been plotted in the nacelle symmetrical plane. These results show a very regular Mach number distribution over the nacelle. It is interesting to observe that there is no great variation in the predicted Mach number field provided by both numerical codes. The predicted results, obtained using  $k-\epsilon$  *realizable* and  $k-\epsilon$  *cubic* model are in very good agreement. Although it is not possible to define which model had a better performance, these results indicate that both turbulence modeling have provided the same behavior to predict this kind of problem. For the two first cases (a) and (b) there are no shock waves on the external fan cowl. The high flow acceleration inside the by pass is typically a function of nozzle pressure ratio.

It's worth to notice the localized interaction between the external and internal nozzle flow at trailing edge of the fan cowl. Figure 6 presents a detailed view of this region with results taken from FLUENT simulations. The results provided by CFD++ simulations show the same behavior. A strong interaction between the external free stream flow and the flow passing inside the engine can be observed. Behind the trailing edge there is a great discrepancy among Mach number values and consequently the static pressure values obtained with the two codes.

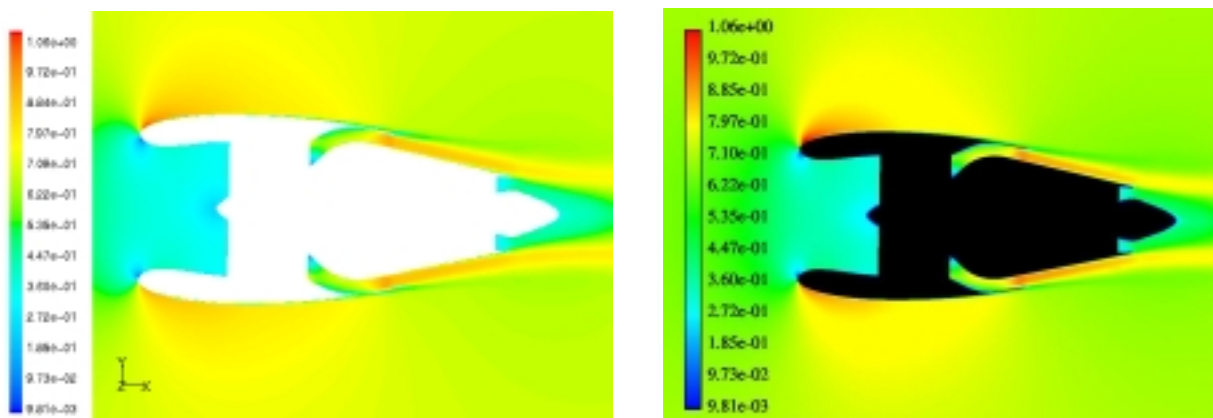
The two last cases (d) and (e) present partially choked and total choked nozzles conditions where the effects of suppression are small/negligible. Once again, these figures show very similar overall results obtained with both codes. It is possible to identify the Mach number greater than unity after the nozzle exit. This trend typical for choked nozzles is well predicted in both simulations.



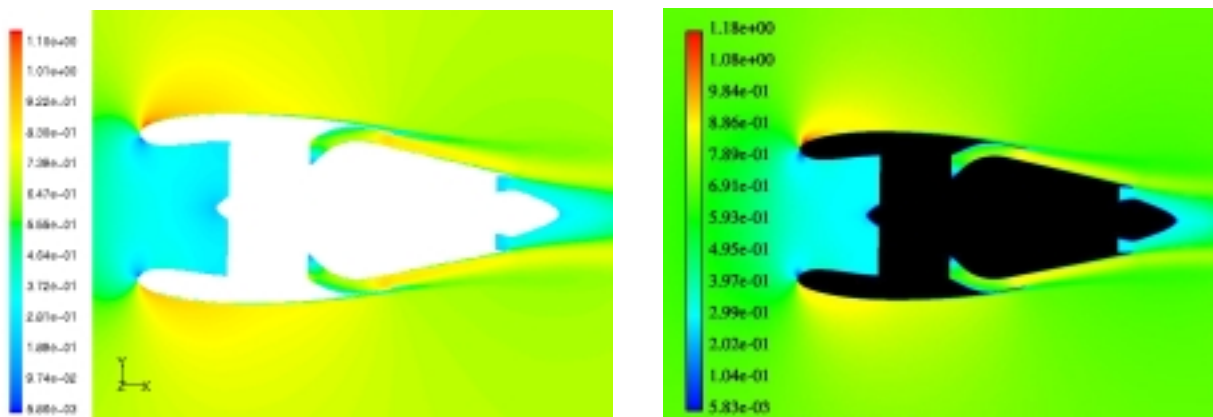
(a)  $M = 0.4$  – Alt = 15000 ft



(b)  $M = 0.6$  – Alt = 15000 ft



(c)  $M = 0.7$  – Alt = 25000 ft



(d)  $M = 0.7$  – Alt = 35000 ft

FLUENT –  $k-\epsilon$  *realizable*

CFD++ -  $k-\epsilon$  *cubic*

**Figure 5.** Mach number distribution at the nacelle symmetrical plane obtained for all analyzed cases with FLUENT and CFD++ solvers.

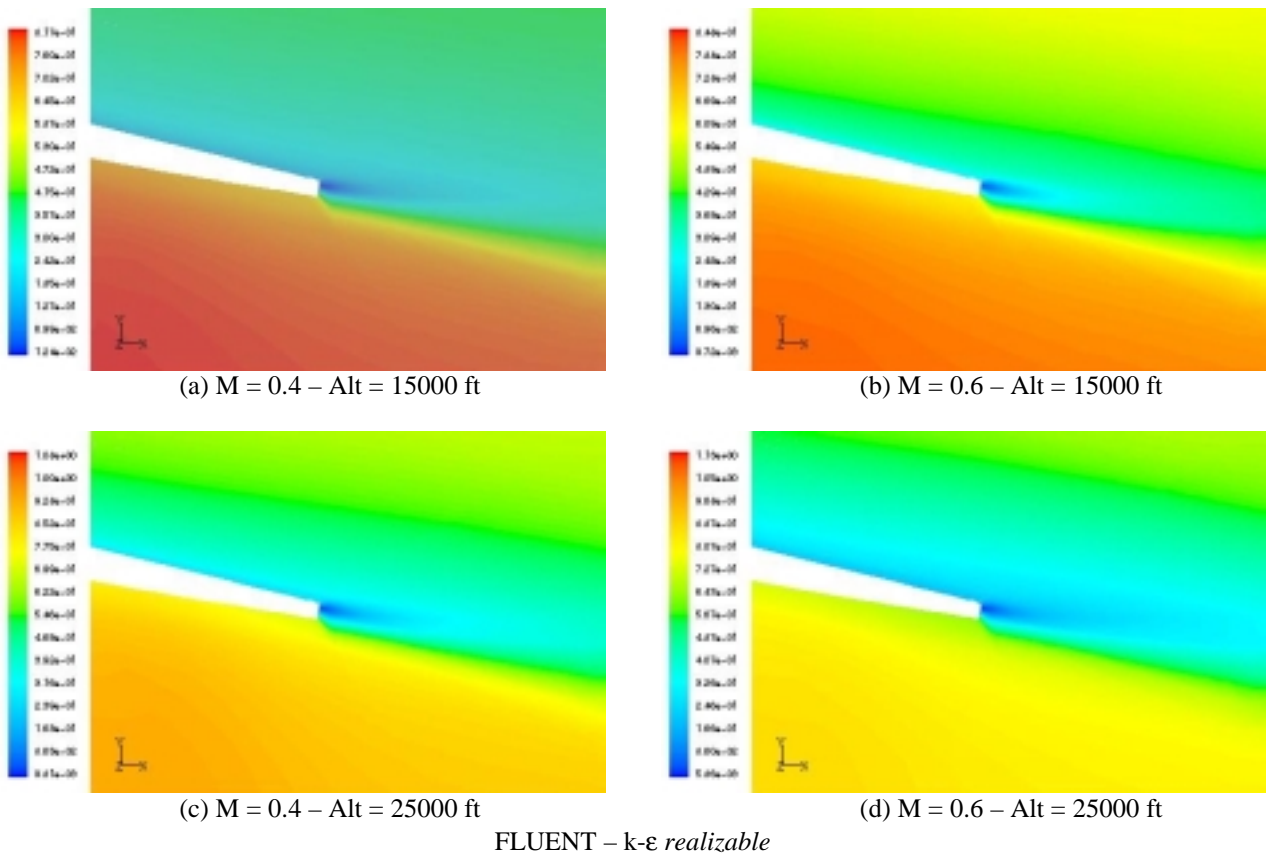


**Figure 6.** Mach number at fan cowl trailing-edge obtained with FLUENT for all analyzed cases.

## 5.2. Pressure Distribution

The leading edge to trailing edge static pressure distributions are shown in the Fig.(7). The static pressure distributions computed with FLUENT and CFD++ are almost identical in all cases, except locally in the regions nearby the leading and trailing edge of fan cowl.

It is interesting to observe the reasonable agreement of the stagnation region at the nacelle intake. After, it is observed a suction peak region where the results from FLUENT and CFD++ rather differ. The minimum difference between the results obtained with both codes in this region was 2% and the maximum was about 28%. Except for the first case, all other ones have shown the same trend with a peak of suction very accentuated provided by FLUENT.

The region of pressure recovery after the fan cowl mid-station is well captured with very good agreement between two codes. No sensitive difference is noted in this region. Finally, the computed points close to the trailing edge have shown some discrepancy between the two codes results, what is expected to influence the suppression calculus. Small changes in the static pressure in this region may cause a considerable impact on the discharge nozzle coefficient and consecutively in the thrust due to suppression.

The differences between the free-stream static pressure and the base pressure at fan cowl for the cases investigated are shown in percentage on Tab. (2). Although good results have been obtained for the general flowfield around the engine the nozzle operating static pressure has not been in good agreement between two codes. Its worth to notice that this effect is very localized at the fan trailing edge and is probably extremely dependent of the fan cowl base's thickness. There are two possible reasons to explain this. One of them is attributed to a coarse mesh refinement in this region, which is not the present situation. Another explanation could be assigned to inability of turbulence models to predict turbulence flows close to base surfaces, including base effects like pressure changes and shear layers.

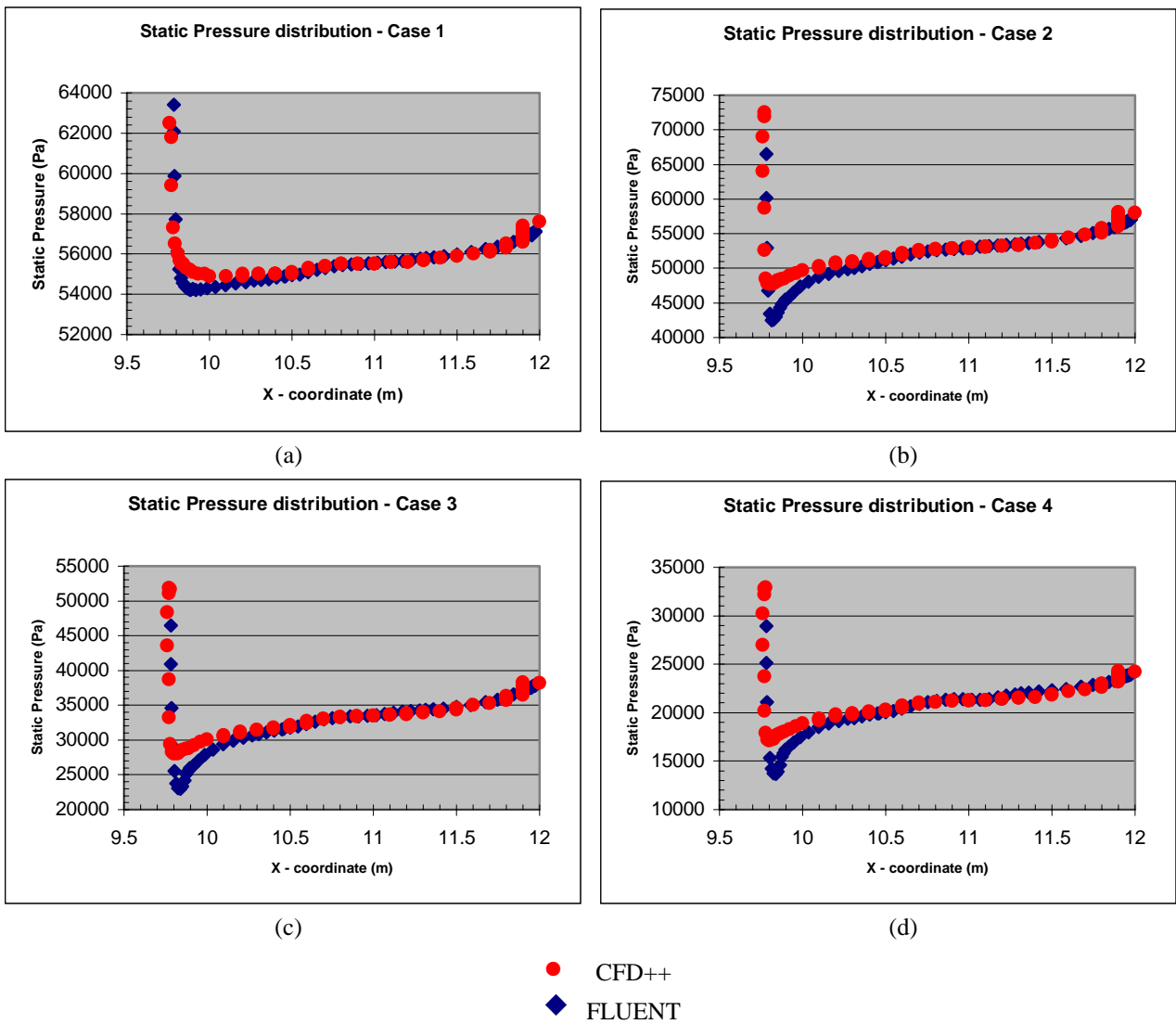


Figure 7. Static pressure distribution over the nacelle.

Table 2. Percentage of Static base pressure in relation with free-stream static pressure.

	FLUENT ( $1-P_{sb19}/P_{s\infty}$ )	CFD++ ( $1-P_{sb19}/P_{s\infty}$ )
Case 1	-0.23%	0.27%
Case 2	-0.53%	0.88%
Case 3	0.37%	1.06%
Case 4	-0.004%	1.03%

### 5.3. Fan Suppression

Table 3 presents the post-processing of results in terms of  $\Delta\%(Q \times CF18)$  according to step 3 of Fig. (4). The negative values indicate that the suppression effect is beneficial increasing thrust. All results indicate very small suppression on the fan nozzle. Exception for the choked case (number 4), where suppression doesn't exist the higher flow suppression estimated was 0,30% in case 2. Typically, only if suppression magnitudes are greater than 1% it is considered to have a strong impact on in-flight thrust determination process and consequently must be taken into account by aircraft manufacturers. The results obtained with CFD++ have shown a better agreement with the engine manufacturer experimental data.

**Table 3.** Suppression effects in terms of  $\Delta\%(Q \times CF18)$ .

	Engine Manufacturer Data	FLUENT	CFD++
Case 1	-0.14 %	+0.07 %	-0.08 %
Case 2	-	+0.18 %	-0.30 %
Case 3	-0.24 %	+0.05 %	+0.15 %
Case 4	-0.8 %	0.00 %	-0.08 %

## 6. Concluding Remarks

In this work a methodology to predict nozzle suppression effects on engine flow and thrust determination was presented. This methodology was applied for the CF34-8E engine of the new Embraer Regional Jet EMB-170.

The CFD results obtained with both FLUENT and CFD++ have shown to be in good agreement. The pressure distribution over the nacelle indicates a difference among 2% to 28% at leading edge of the fan cowl. In counterpart it is observed a reasonable agreement for the recovery pressure along the nacelle. A comparison of the static base pressure calculated at the trailing-edge of fan cowl has shown different results for all cases. Both experimental and numerical results indicate negligible suppression effects, smaller than 0,3% in the unchoked cases.

## 7. References

- Goldberg, U., Peroomian, O., Palaniswamy, S. and Chakravarthy, S., Anisotropic k-e model for adverse pressure gradient flow, AIAA Paper 99-0152 (1999).
- Lien, F.S. and Leschziner, M.A., Low-Reynolds-number eddy-viscosity modeling based on non-linear stress-strain/vorticity relations. In: Rodi, W. and Bergeles, G. (eds.), Engineering Turbulence Modeling and Experiments 3, Elsevier, Amsterdam (1996).
- Reynolds, W., C., Reynolds Fundamentals of turbulence for turbulence modeling and simulation, Lecture Notes for Von Karman Institute Agard Report No. 755, 1987.
- SAE Report Air 1703, "In Flight Thrust Determination", 1985
- Santos, G., D., In-flight thrust determination and uncertainty analysis for turbofan engines, Master thesis, (2002).
- Shih, T.H., Lumley, J.L. and Zhou, J., A realizable Reynolds stress algebraic equation model. NASA TM-105993 (1993).
- T-H. Shih, W. W. Liou, A. Shabbir, and J. Zhu. A New k-Eddy-Viscosity Model for High Reynolds Number Turbulent Flows - Model Development and Validation. Computers Fluids, 24(3):227-238, 1995.
- Tulapurkara, E. G., Turbulence Models for the Computation of Flow Past Airplanes, Prog. Aerospace Sci. Vol. 33, pp. 781-165, 1997.
- Williams, D., Airframe Engine Integration, Lecture notes, Cranfield University, Cranfield (1996).